

Recent $B \rightarrow X_s \gamma$ and $B \rightarrow X \ell \ell$ Results from B Factories

L. Sun (on behalf of the BABAR and Belle collaborations)
University of Cincinnati, Cincinnati OH 45221, USA

In this talk, a wide range of recently published results on rare B decays from BABAR and Belle are covered. The decays of $B \rightarrow X_s \gamma$, $B \rightarrow K^{(*)} \ell^+ \ell^-$, and lepton-number violation in B decays are measured for new physics searches.

I. INTRODUCTION

By 2008 and 2010, BABAR and Belle completed data-taking respectively. Both B factories produced $B\bar{B}$ pairs at the $\Upsilon(4S)$ resonance with asymmetric-energy e^+e^- colliders. These $B\bar{B}$ pairs were collected with BABAR and Belle detectors. Both detectors share similar designs and provide good discrimination on charged particles, especially for K^\pm/π^\pm . Muons are also differentiated from charged hadrons. High-energy photons and electrons are precisely measured with electro-magnetic calorimeters in both detectors.

The BABAR and Belle collaborations continue to produce interesting results on rare B decays. Based on 471 million $B\bar{B}$ pairs from BABAR this talk presents $b \rightarrow s \gamma$ transition rates and photon energy spectrum using a sum of exclusive modes, rates and asymmetries in exclusive $B \rightarrow K^* \ell^+ \ell^-$ decays, and a search for lepton-number violation (LNV) processes in $B^+ \rightarrow K^- \ell^+ \ell^+$ decays[23]. In addition, this talk presents a search for LNV processes in $B^+ \rightarrow D^- \ell^+ \ell^+$ decays based on 773 million $B\bar{B}$ pairs from Belle.

II. $B \rightarrow X_s \gamma$ TRANSITION RATES AND PHOTON ENERGY SPECTRUM WITH A SUM OF EXCLUSIVE MODES

The $b \rightarrow s \gamma$ transitions are flavor-changing neutral-current (FCNC) processes and forbidden at tree level in the Standard Model (SM). The leading-order radiative penguin diagram for this type of transition is shown in Figure 1. For photon energy $E_\gamma > 1.6$ GeV, the SM-based prediction for the decay rate is at $\mathcal{B}(\bar{B} \rightarrow X_s \gamma) = (3.15 \pm 0.23) \times 10^{-4}$ [1], with X_s as the hadronic final state with strangeness. This prediction is in good agreement with the current world average of experimental results at $\mathcal{B}(\bar{B} \rightarrow X_s \gamma) = (3.55 \pm 0.25 \pm 0.09) \times 10^{-4}$ for the same photon energy cutoff at $E_\gamma > 1.6$ GeV [2]. Here the second uncertainty comes from the extrapolation of the photon energy shape function from the experimental photon energy to the 1.6 GeV cutoff. New physics beyond the SM may enter the radiative loop of $b \rightarrow s \gamma$ and alter the decay rate significantly. Therefore comparing the experimental results and SM-based predictions provides a good test of the SM. Furthermore, the photon energy spectrum is important for us to understand the b quark momentum distribution inside the B meson.

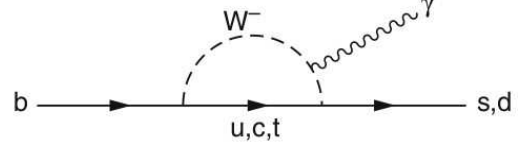


FIG. 1: The leading order Feynman diagram for the transition $b \rightarrow (s/d) \gamma$ in the SM. [3]

The shape of this distribution is a critical input to the determination of the CKM matrix element $|V_{ub}|$ in inclusive charmless semileptonic B decays. The measured energy spectrum can be fit to different models in order to find the best values of m_b and μ_π^2 as the heavy quark effective theory (HQET) parameters.

This BABAR analysis [3] reconstructs the X_s system in 38 different exclusive final states listed in Table I. With the reconstructed X_s system, the energy of the transition photon in the B rest frame E_γ^B is thus accessible through:

$$E_\gamma^B = \frac{m_B^2 - m_{X_s}^2}{2m_B}, \quad (1)$$

where m_B and m_{X_s} are the invariant masses of the B meson and of the X_s hadronic system, respectively.

In each event, this analysis requires at least one photon candidate with $1.6 < E_\gamma^* < 3.0$ GeV in the center-of-mass (CM) frame. This analysis also requires m_{X_s} to be within a range of 0.6 and 2.8 GeV/ c^2 , and divides this range into 18 bins. These 18 m_{X_s} bins include 14 bins each with a width of 100 MeV/ c^2 for $m_{X_s} < 2.0$ GeV/ c^2 , and 4 bins each with a width of 200 MeV/ c^2 for $m_{X_s} \geq 2.0$ GeV/ c^2 . Common to all other BABAR analyses, the beam-energy substituted mass $m_{ES} = \sqrt{E_{\text{beam}}^{*2} - p_B^{*2}}$ is defined, where E_{beam}^* and p_B^* are the beam energy and the B meson momentum in the CM frame, respectively. In each m_{X_s} bin, the m_{ES} distribution is fit to extract the signal yield. An example of the m_{ES} fit for $1.4 < m_{X_s} < 1.5$ GeV/ c^2 is shown in Fig. 2.

Figure 3 shows the measured partial branching fractions in the 18 m_{X_s} bins, as well as in the corresponding E_γ bins. The measured m_{X_s} spectrum is fit with two different models: the “kinetic model” [4] and “shape function model” [5], to find the best values for m_b and μ_π^2 as summarized in Table II. These numbers are compatible with the world averages for these two models [2] also listed in Tables II. Figure 3

TABLE I: The 38 final states for $B \rightarrow X_s \gamma$ used in this analysis. Here K_s^0 is reconstructed through $K_s^0 \rightarrow \pi^+ \pi^-$. [3]

Mode No.	Final State	Mode No.	Final State
1	$K_s^0 \pi^+ \gamma$	20	$K_s^0 \pi^+ \pi^- \pi^+ \pi^- \gamma$
2	$K^+ \pi^0 \gamma$	21	$K^+ \pi^+ \pi^- \pi^- \pi^0 \gamma$
3	$K^+ \pi^- \gamma$	22	$K_s^0 \pi^+ \pi^- \pi^0 \pi^0 \gamma$
4	$K_s^0 \pi^0 \gamma$	23	$K^+ \eta \gamma$
5	$K^+ \pi^+ \pi^- \gamma$	24	$K_s^0 \eta \gamma$
6	$K_s^0 \pi^+ \pi^0 \gamma$	25	$K_s^0 \eta \pi^+ \gamma$
7	$K^+ \pi^0 \pi^0 \gamma$	26	$K^+ \eta \pi^0 \gamma$
8	$K_s^0 \pi^+ \pi^- \gamma$	27	$K^+ \eta \pi^- \gamma$
9	$K^+ \pi^- \pi^0 \gamma$	28	$K_s^0 \eta \pi^0 \gamma$
10	$K_s^0 \pi^+ \pi^0 \gamma$	29	$K^+ \eta \pi^+ \pi^- \gamma$
11	$K_s^0 \pi^+ \pi^- \pi^+ \gamma$	30	$K_s^0 \eta \pi^+ \pi^0 \gamma$
12	$K^+ \pi^+ \pi^- \pi^0 \gamma$	31	$K_s^0 \eta \pi^+ \pi^- \gamma$
13	$K_s^0 \pi^+ \pi^0 \pi^0 \gamma$	32	$K^+ \eta \pi^- \pi^0 \gamma$
14	$K^+ \pi^+ \pi^- \pi^- \gamma$	33	$K^+ K^- K^+ \gamma$
15	$K_s^0 \pi^0 \pi^+ \pi^- \gamma$	34	$K^+ K^- K_s^0 \gamma$
16	$K^+ \pi^- \pi^0 \pi^0 \gamma$	35	$K^+ K^- K_s^0 \pi^+ \gamma$
17	$K^+ \pi^+ \pi^- \pi^+ \pi^- \gamma$	36	$K^+ K^- K^+ \pi^0 \gamma$
18	$K_s^0 \pi^+ \pi^- \pi^+ \pi^0 \gamma$	37	$K^+ K^- K^+ \pi^- \gamma$
19	$K^+ \pi^+ \pi^- \pi^0 \pi^0 \gamma$	38	$K^+ K^- K_s^0 \pi^0 \gamma$

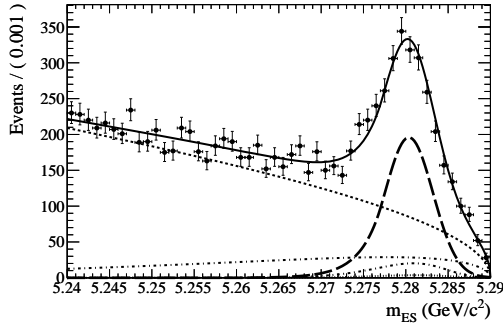


FIG. 2: BABAR: m_{ES} fit example in the region $1.4 < m_{X_s} < 1.5$ GeV/c^2 . Shown are data (points with error bars) along with the total fit (solid curve), signal (thick dashed curve), and different background contributions (other curves, see Ref. [3] for detailed description).

also shows the fit with the kinetic model as an example. By combining the partial branching fraction results, the total branching fraction for $E_\gamma > 1.9$ GeV is $\mathcal{B}(\bar{B} \rightarrow X_s \gamma) = (3.29 \pm 0.19 \pm 0.48) \times 10^{-4}$, where the first and second uncertainties are statistical and systematic, respectively.

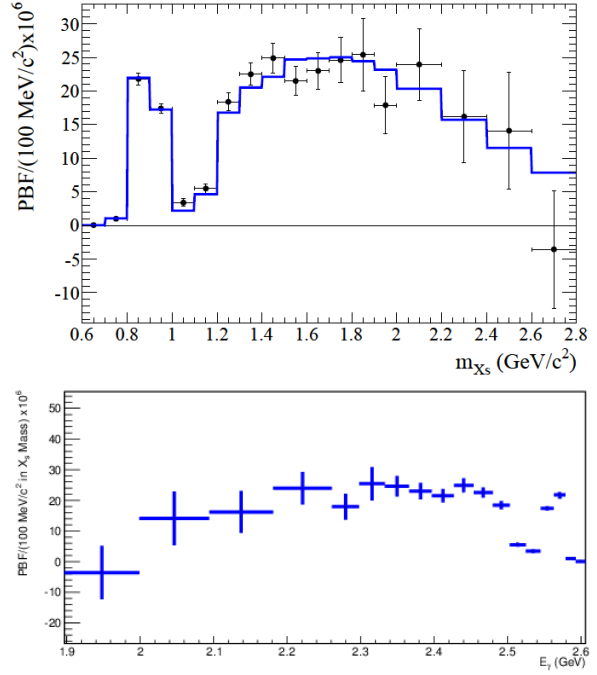


FIG. 3: BABAR: Top: Measured partial branching fractions (points with error bars) in the 18 m_{X_s} bins, with the spectrum fit using the kinetic model (solid line). Bottom: Measured partial branching fractions (points with error bars) in the corresponding photon energy bins. All the error bars shown here include the statistical and systematic uncertainties added in quadrature. [3]

TABLE II: The best fit HQET parameter values based on the measured m_{X_s} spectrum, are compared to the world averages (“HFAG”). [3]

	Kinetic model	Shape function model
m_b (GeV/c^2)	$4.568^{+0.038}_{-0.036}$	$4.579^{+0.032}_{-0.029}$
HFAG:	4.591 ± 0.031	$4.620^{+0.039}_{-0.032}$
μ_π^2 (GeV^2)	$0.450^{+0.054}_{-0.054}$	$0.257^{+0.034}_{-0.039}$
HFAG:	0.454 ± 0.038	$0.288^{+0.054}_{-0.074}$

III. EXCLUSIVE $B \rightarrow K^{(*)} \ell^+ \ell^-$ DECAYS

Similar to $b \rightarrow s \gamma$, the FCNC $b \rightarrow s \ell^+ \ell^-$ processes are also forbidden at tree level in the SM. The $B \rightarrow K^{(*)} \ell^+ \ell^-$ decays are allowed in the loop and box diagrams as shown in Fig. 4 with branching fractions at about 10^{-6} . The effective Hamiltonian for these decays factorizes short-distances contributions represented by the Wilson coefficients from long-distance effects. Three effective Wilson coefficients are relevant here: C_7^{eff} from the electromagnetic penguin diagram, C_9^{eff} and C_{10}^{eff} from the vector part and the axial-vector part of the Z penguin and $W^+ W^-$ box diagrams, respectively [6]. New physics may bring in

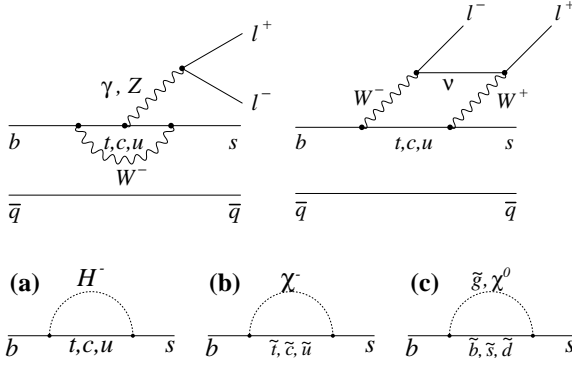


FIG. 4: Top: Lowest-order Feynman diagrams for $b \rightarrow s \ell^+ \ell^-$ in the SM. Bottom: Examples of new physics loop contributions to $b \rightarrow s \ell^+ \ell^-$: (a) charged Higgs (H^-); (b) squark ($\tilde{t}, \tilde{c}, \tilde{u}$) and chargino (χ^-); (c) squark ($\tilde{b}, \tilde{s}, \tilde{d}$) and gluino (\tilde{g})/neutralino (χ^0). [11]

new loops involving particles such as charged Higgs, squarks, neutralinos, and charginos particles as depicted in the bottom of Figure 4. These loop contributions may be comparable to the SM ones, and alter the effective Wilson coefficient values from their SM expectations [7].

In this *BABAR* analysis, $B \rightarrow K^{(*)} \ell^+ \ell^-$ signal events are reconstructed in eight final states with an $e^+ e^-$ or $\mu^+ \mu^-$ pair, and a K_s^0 , K^+ , $K^{*+} (\rightarrow K_s^0 \pi^+)$, or $K^{*0} (\rightarrow K^+ \pi^-)$, where a K_s^0 candidate is reconstructed in the $\pi^+ \pi^-$ final state. Another final state $K^+ \pi^0 e^+ e^-$ is included only for the $K^* \ell^+ \ell^-$ angular measurements introduced in Sect. III B. Selected K^* candidates are also required to have an invariant mass of $0.72 < m_{K\pi} < 1.10$ GeV/c^2 . The measurements are performed in six bins of di-lepton mass squared $s \equiv m_{\ell\ell}^2$: $0.1 \leq s < 2.0$ GeV^2/c^4 , $2.0 \leq s < 4.3$ GeV^2/c^4 , $4.3 \leq s < 8.1$ GeV^2/c^4 , $10.1 \leq s < 12.9$ GeV^2/c^4 , $14.2 \leq s < 16.0$ GeV^2/c^4 , and $s \geq 16.0$ GeV^2/c^4 . In the analysis, two s regions are vetoed to minimize the J/ψ and $\psi(2S)$ contributions. The binning choices are largely consistent with those used in the Belle [8], CDF [9], and LHCb [10] experiments. An example m_{ES} fit to extract signal $K \ell^+ \ell^-$ events is depicted in Fig. 5. The experimental details are presented in Ref. [11].

A. Rates and Rate Asymmetries

The measured total branching fractions are:

$$\begin{aligned} \mathcal{B}(B \rightarrow K \ell^+ \ell^-) &= (4.7 \pm 0.6 \pm 0.2) \times 10^{-7}, \\ \mathcal{B}(B \rightarrow K^* \ell^+ \ell^-) &= (10.2_{-1.3}^{+1.4} \pm 0.5) \times 10^{-7}, \end{aligned}$$

where the first and second uncertainties are statistical and systematic, respectively. In Fig. 6, the measured total branching fraction results agree well with the

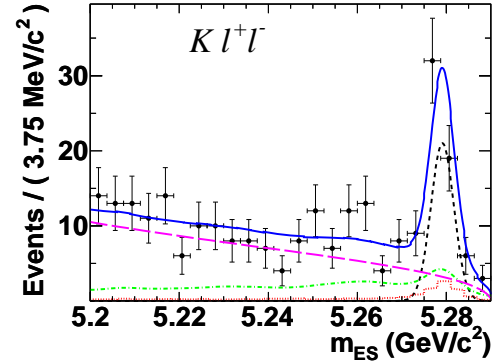


FIG. 5: *BABAR*: Example m_{ES} fit in the region $10.1 \leq s < 12.9$ GeV^2/c^4 for $B \rightarrow K \ell^+ \ell^-$. Data (points with error bars) are shown along with the total fit (solid curve), signal (short-dashed curve), and different background contributions (other curves, see Ref. [11] for detailed description).

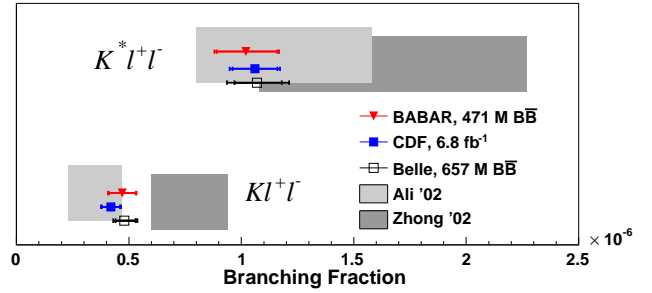


FIG. 6: *BABAR*: Total branching fractions for $K \ell^+ \ell^-$ and $K^* \ell^+ \ell^-$ compared with Belle [8] and CDF [9] measurements and with predictions from the Ali *et al.* [12], and Zhong *et al.* [13] models. [11]

results from the Belle and CDF experiments [8, 9], as well as two sets of SM-based predictions [12, 13]. Figure 7 shows the *BABAR* partial branching fraction results in agreement with the Belle, CDF, and LHCb results [8–10]. These *BABAR* results are also consistent with the SM-based predictions [12, 14].

In the SM, the direct CP asymmetry

$$\mathcal{A}_{CP}^{K^{(*)}} \equiv \frac{\mathcal{B}(\overline{B} \rightarrow \overline{K}^{(*)} \ell^+ \ell^-) - \mathcal{B}(B \rightarrow K^{(*)} \ell^+ \ell^-)}{\mathcal{B}(\overline{B} \rightarrow \overline{K}^{(*)} \ell^+ \ell^-) + \mathcal{B}(B \rightarrow K^{(*)} \ell^+ \ell^-)} \quad (2)$$

and lepton flavor ratio

$$\mathcal{R}_{K^{(*)}} \equiv \frac{\mathcal{B}(B \rightarrow K^{(*)} \mu^+ \mu^-)}{\mathcal{B}(B \rightarrow K^{(*)} e^+ e^-)} \quad (3)$$

are expected to be very close to zero and one, respectively. Our measured \mathcal{A}_{CP} and $\mathcal{R}_{K^{(*)}}$ results agree with the SM expectations, as shown in Fig 8.

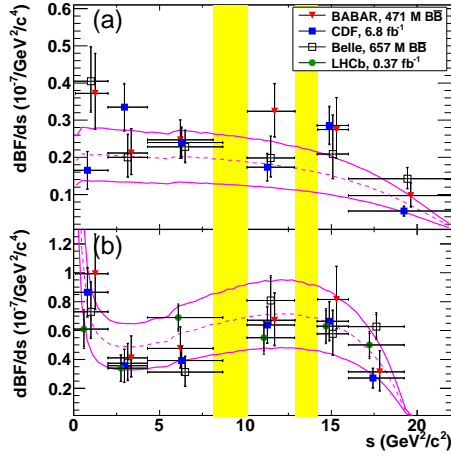


FIG. 7: *BABAR*: Partial branching fractions for (a) $K^+ \ell^+ \ell^-$ and (b) $K^* \ell^+ \ell^-$ as a function of s showing *BABAR* measurements, Belle measurements [8], CDF measurements [9], LHCb measurements [10], and the SM prediction from the Ali *et al.* model [12] with $B \rightarrow K^{(*)}$ form factors [14] (magenta dashed lines). The magenta solid lines show the theory uncertainties. The vertical yellow shaded bands show the vetoed s regions around the J/ψ and $\psi(2S)$ resonances. [11]

The CP -averaged isospin asymmetry is defined as:

$$\mathcal{A}_I^{K^{(*)}} \equiv \frac{\mathcal{B}(B^0 \rightarrow K^{(*)0} \ell^+ \ell^-) - r_\tau \mathcal{B}(B^+ \rightarrow K^{(*)+} \ell^+ \ell^-)}{\mathcal{B}(B^0 \rightarrow K^{(*)0} \ell^+ \ell^-) + r_\tau \mathcal{B}(B^+ \rightarrow K^{(*)+} \ell^+ \ell^-)}, \quad (4)$$

where $r_\tau \equiv \tau_{B^0}/\tau_{B^+} = 1/(1.071 \pm 0.009)$ is the ratio of B^0 and B^+ lifetimes [15]. In the SM, the isospin asymmetries are expected to be at the level of a few percent [7]. Figure 9 shows the *BABAR* isospin asymmetry results in agreement with the earlier Belle results [8]. The corresponding LHCb results are presented in a separate FPCP 2012 talk [16]. This *BABAR* analysis also measure below the J/ψ resonance ($0.1 < s < 8.12 \text{ GeV}^2/c^4$):

$$\begin{aligned} \mathcal{A}_I^{\text{low}}(B \rightarrow K \ell^+ \ell^-) &= -0.58_{-0.37}^{+0.29} \pm 0.02, \\ \mathcal{A}_I^{\text{low}}(B \rightarrow K^* \ell^+ \ell^-) &= -0.25_{-0.17}^{+0.20} \pm 0.03, \end{aligned}$$

where the first and second uncertainties are statistical and systematic, respectively. The above two results are consistent with the SM predictions at 2.1σ and 1.2σ significance levels, respectively. They also agree with the corresponding Belle results [8].

B. Angular Asymmetries

For the angular observables in $B \rightarrow K^* \ell^+ \ell^-$, two angles are relevant here: θ_K as the angle between the K and the B in the K^* rest frame, and θ_ℓ as the angle between the ℓ^+ (ℓ^-) and the B (\bar{B}) in the $\ell^+ \ell^-$ rest

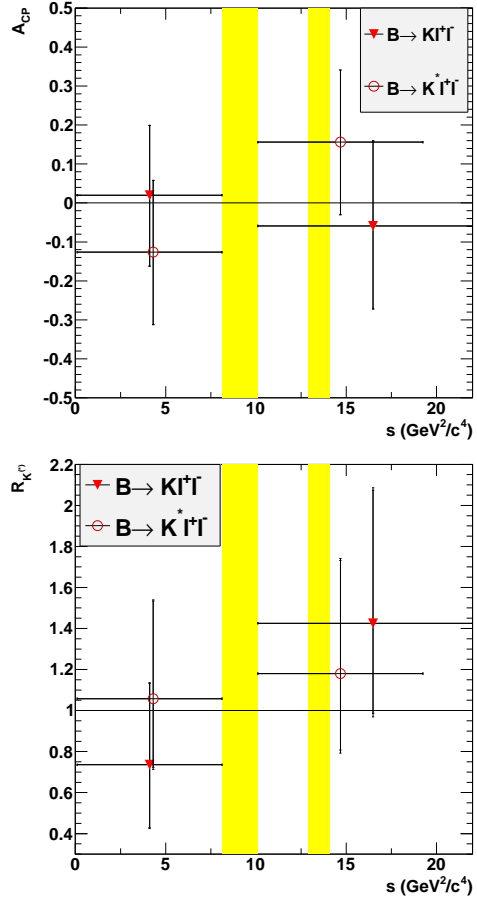


FIG. 8: *BABAR*: (top) CP asymmetries \mathcal{A}_{CP} and (bottom) $R_{K^{(*)}}$ in two s regions for $K \ell^+ \ell^-$ and $K^* \ell^+ \ell^-$. The vertical yellow shaded bands show the vetoed s regions around the J/ψ and $\psi(2S)$. [11]

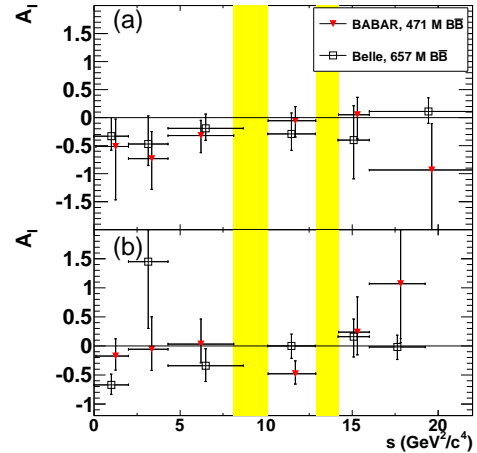


FIG. 9: *BABAR*: Isospin asymmetry \mathcal{A}_I for the (a) $K \ell^+ \ell^-$ and (b) $K^* \ell^+ \ell^-$ modes as a function of s , in comparison to results from Belle [8]. The vertical yellow shaded bands show the vetoed s regions around the J/ψ and $\psi(2S)$ resonance. [11]

frame. The fraction of the K^* longitudinal F_L and the lepton forward-backward asymmetry \mathcal{A}_{FB} are related to the distributions of $\cos\theta_K$ and $\cos\theta_\ell$ in the signal $B \rightarrow K^*\ell^+\ell^-$ decays through:

$$\begin{aligned} \frac{1}{\Gamma} \frac{d\Gamma}{d\cos\theta_K} &= \frac{3}{2} F_L \cos^2\theta_K + \frac{3}{4} (1 - F_L) (1 - \cos^2\theta_K), \\ \frac{1}{\Gamma} \frac{d\Gamma}{d\cos\theta_\ell} &= \frac{3}{4} F_L (1 - \cos^2\theta_\ell) + \\ &\quad \frac{3}{8} (1 - F_L) \cdot (1 + \cos^2\theta_\ell) + \mathcal{A}_{FB} \cos\theta_\ell. \end{aligned}$$

The values of F_L and \mathcal{A}_{FB} can thus be extracted through the fits to these angular distributions. Both F_L and \mathcal{A}_{FB} are well predicted in the SM, and follow distinct patterns as functions of s [12, 14, 17]. Starting from $s \rightarrow 0$, where C_7^{eff} dominates, the SM value of \mathcal{A}_{FB} is negative at very low s , then cross the zero axis at $s \sim 4 \text{ GeV}^2/c^4$. At large s above the J/ψ resonance, the SM value of \mathcal{A}_{FB} is expected to be large and positive due to the domination of the product of C_9^{eff} and C_{10}^{eff} . F_L is only sensitive to the sign of C_7^{eff} , while \mathcal{A}_{FB} is sensitive to both the sign of C_7^{eff} and that of $C_9^{\text{eff}} \cdot C_{10}^{\text{eff}}$.

Figure 10 shows the BABAR F_L and \mathcal{A}_{FB} results for the $B^+ \rightarrow K^{*+}\ell^+\ell^-$ modes, $B^0 \rightarrow K^{*0}\ell^+\ell^-$ modes, and all $B \rightarrow K^*\ell^+\ell^-$ modes combined, in the six s bins. The F_L and \mathcal{A}_{FB} results for the combined $B \rightarrow K^*\ell^+\ell^-$ are consistent with the most recent results from Belle [8], CDF [18], and LHCb [10], as well as the SM predictions [12, 14, 17]. Still some discrepancies with the SM are noticeable in the low s bins below J/ψ for the $B^+ \rightarrow K^{*+}\ell^+\ell^-$ modes.

IV. SEARCH FOR LEPTON-NUMBER VIOLATING PROCESSES

In the SM with massless neutrinos, it is expected that the lepton number L is conserved in low-energy collisions and decays. However, the observation of neutrino oscillation indicates that neutrinos possess non-zero masses. If the neutrino masses are of Majorana type, *i.e.* each neutrino is its own anti-particle, the L violation will be possible. Figure 11 shows two different types of $\Delta L = 2$ processes involving Majorana neutrinos: $B^+ \rightarrow D^-\ell^+\ell^+$, and $B^+ \rightarrow (\pi^-/K^-)\ell^+\ell^+$. The search on these decays is an alternative approach to the search for neutrinoless double-beta decay.

A. Search for $B^+ \rightarrow D^-\ell^+\ell^+$

In this Belle analysis on $B^+ \rightarrow D^-\ell^+\ell^+$ [19], D^- meson is reconstructed through $D^- \rightarrow K^+\pi^-\pi^-$, and $\ell^+\ell^+$ is either e^+e^+ , $\mu^+\mu^+$, or $e^+\mu^+$. Two kinematic variables are defined to identify signal B decays: the

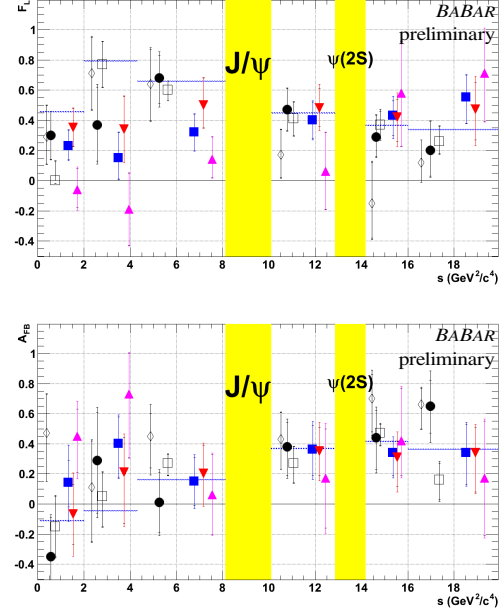


FIG. 10: BABAR: Summary on (top) F_L and (bottom) \mathcal{A}_{FB} as a function of s for $B \rightarrow K^*\ell^+\ell^-$. Our results for $B^+ \rightarrow K^{*+}\ell^+\ell^-$ (\blacktriangle), $B^0 \rightarrow K^{*0}\ell^+\ell^-$ (\blacktriangledown), and all $B \rightarrow K^*\ell^+\ell^-$ modes combined (\blacksquare) are compared to the results from Belle (\diamond), CDF (\bullet), and LHCb (\square), as well as the SM predictions (blue dashed lines).

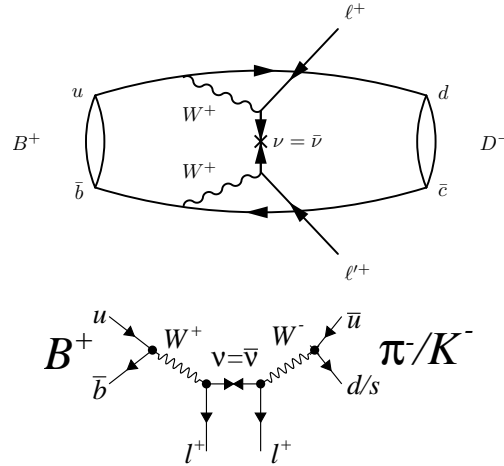


FIG. 11: Possible Feynman diagrams for the decays (top) $B^+ \rightarrow D^-\ell^+\ell^+$ [19] and (bottom) $B^+ \rightarrow (\pi^-/K^-)\ell^+\ell^+$ [20].

energy difference $\Delta E = E_B^* - E_{\text{beam}}^*$ between the beam energy and the B meson energy in the CM frame, and the beam-energy-constrained B meson mass M_{bc} , which is identical to m_{ES} used in the BABAR experiment. A two-dimensional (2D) fit is performed to the $M_{\text{bc}}-\Delta E$ distribution for signal extraction. Figure 12 shows the fit projections in the $D^-\mu^+\mu^+$ mode. The

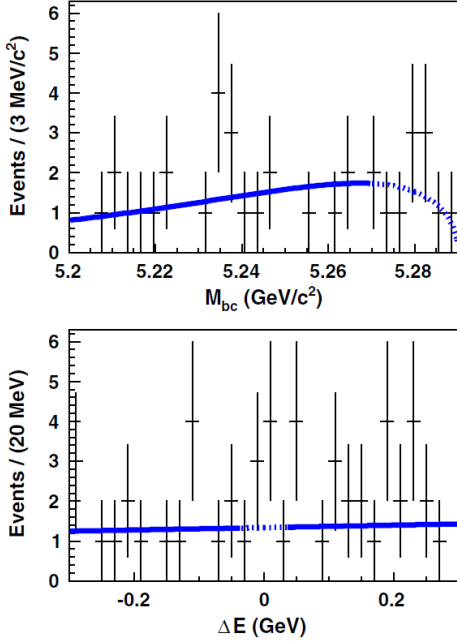


FIG. 12: Belle: The 2D fit projections and data for (top) M_{bc} and (bottom) ΔE in the $D^- \mu^+ \mu^+$ mode. See Ref.[19] for detailed description.

TABLE III: The 90% C.L. upper limit (U.L.) on the branching fraction of $B^+ \rightarrow D^- \ell^+ \ell^+$. Here ϵ is the signal reconstruction efficiency, N_{obs} is the number of events in the signal region, $N_{\text{exp}}^{\text{bkg}}$ is the expected number of background events in the signal region. The efficiencies shown in the table do not include the branching fraction of the D^- decay. [19]

Mode	ϵ [%]	N_{obs}	$N_{\text{exp}}^{\text{bkg}}$	U.L. [10^{-6}]
$B^+ \rightarrow D^- e^+ e^+$	1.2	0	0.18 ± 0.13	< 2.6
$B^+ \rightarrow D^- e^+ \mu^+$	1.3	0	0.83 ± 0.29	< 1.8
$B^+ \rightarrow D^- \mu^+ \mu^+$	1.9	0	1.44 ± 0.43	< 1.0

90% C.L. upper limits on the branching fractions for different $B^+ \rightarrow D^- \ell^+ \ell^+$ modes are $(1.0 - 2.6) \times 10^{-6}$ as summarized in Table III.

B. Search for $B^+ \rightarrow h^- \ell^+ \ell^+$

In this *BABAR* analysis [20], the search is performed in four different final states: $\pi^- e^+ e^+$, $K^- e^+ e^+$, $\pi^- \mu^+ \mu^+$, and $K^- \mu^+ \mu^+$. Since these final states are very similar to the ones in the $B \rightarrow K^{(*)} \ell^+ \ell^-$ analysis described in the previous section, both analyses also share similar event selection techniques. As no significant evidence for signal events could be found, this analysis sets the 90% C.L. upper limits on the branching fractions for the four modes as summarized in Table IV. These results are comparable to the LHCb re-

TABLE IV: 90% C.L. upper limits on the branching fractions (\mathcal{B}_{UL}) for the four measured B decays. [20]

Mode	$\mathcal{B}(\times 10^{-8})$	$\mathcal{B}_{UL}(\times 10^{-8})$
$B^+ \rightarrow \pi^- e^+ e^+$	$0.27^{+1.1}_{-1.2} \pm 0.1$	2.3
$B^+ \rightarrow K^- e^+ e^+$	$0.49^{+1.3}_{-0.8} \pm 0.1$	3.0
$B^+ \rightarrow \pi^- \mu^+ \mu^+$	$0.03^{+5.1}_{-3.2} \pm 0.6$	10.7
$B^+ \rightarrow K^- \mu^+ \mu^+$	$0.45^{+3.2}_{-2.7} \pm 0.4$	6.7

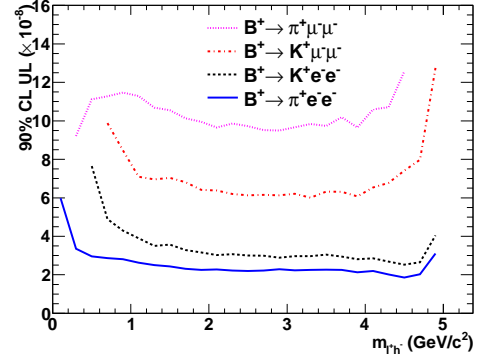


FIG. 13: *BABAR*: 90% C.L. upper limits on the branching fraction as a function of $m_{\ell^+ \ell^-}$ for $B^+ \rightarrow \pi^- e^+ e^+$ (blue solid line), $B^+ \rightarrow K^- e^+ e^+$ (black dashed line), $B^+ \rightarrow \pi^- \mu^+ \mu^+$ (red dash-dotted line), and $B^+ \rightarrow K^- \mu^+ \mu^+$ (magenta dotted line). [20]

sults [21] and provide much more stringent constraints than the CLEO results [22]. The upper limits on the electron channels are also the most stringent ones to date. Furthermore, Figure 13 shows the 90% C.L. upper limit on the branching fraction as a function of the invariant mass $m_{\ell^+ \ell^-}$. If an exchange of the Majorana neutrino occurs in the decay $B^+ \rightarrow h^- \ell^+ \ell^+$ as illustrated in the left diagram of Fig. 11, $m_{\ell^+ \ell^-}$ could be interpreted as the Majorana neutrino mass.

V. CONCLUSION

Both the *BABAR* and Belle experiments are still actively producing interesting results based on their full data sets. As B factories, they are capable of inclusive analyses on the $b \rightarrow s \gamma$ and $b \rightarrow s \ell^+ \ell^-$ processes. This report covers new results on rare B decay channels from *BABAR* and Belle. Generally all these results are found to be consistent with the SM predictions, though some discrepancies exist for the angular asymmetries in the channel $B \rightarrow K^{(*)} \ell^+ \ell^-$. The current B factory results are limited by low statistics, therefore we have to rely on LHCb and future B factories to continue new physics searches in these decay channels.

Acknowledgments

the conference organizers for their great work.

The author is supported by the United States National Science Foundation grants. Special thanks to

-
- [1] M. Misiak, H. M. Asatrian, K. Bieri, M. Czakon, A. Czarnecki, T. Ewerth, A. Ferroglia and P. Gambino *et al.*, Phys. Rev. Lett. **98**, 022002 (2007).
 - [2] D. Asner *et al.* [Heavy Flavor Averaging Group Collaboration], arXiv:1010.1589 [hep-ex].
 - [3] J. P. Lees *et al.* [BABAR Collaboration], arXiv:1207.2520 [hep-ex].
 - [4] D. Benson, I. I. Bigi and N. Uraltsev, Nucl. Phys. B **710**, 371 (2005).
 - [5] B. O. Lange, M. Neubert and G. Paz, Phys. Rev. D **72**, 073006 (2005).
 - [6] G. Buchalla, A. J. Buras, and M. E. Lautenbacher, Rev. Mod. Phys. **68**, 1125 (1996).
 - [7] T. Feldmann and J. Matias, JHEP **0301**, 074 (2003).
 - [8] J.-T. Wei *et al.* [Belle Collaboration], Phys. Rev. Lett. **103**, 171801 (2009).
 - [9] T. Aaltonen *et al.* [CDF Collaboration], Phys. Rev. Lett. **107**, 201802 (2011).
 - [10] R. Aaij *et al.* [LHCb Collaboration], Phys. Rev. Lett. **108**, 181806 (2012).
 - [11] J. P. Lees *et al.* [BABAR Collaboration], Phys. Rev. D **86**, 032012 (2012).
 - [12] A. Ali, E. Lunghi, C. Greub, and G. Hiller, Phys. Rev. D **66**, 034002 (2002).
 - [13] M. Zhong, Y.-L. Wu, and W.-Y. Wang, Int. J. Mod. Phys. A **18**, 1959 (2003).
 - [14] P. Ball and R. Zwicky, Phys. Rev. D **71**, 014015 (2005); Phys. Rev. D **71**, 014029 (2005).
 - [15] K. Nakamura *et al.* [Particle Data Group], J. Phys. G **37** (2010) 075021.
 - [16] N. Serra, arXiv:1208.3987 [hep-ex].
 - [17] A. Ali, P. Ball, L. T. Handoko and G. Hiller, Phys. Rev. D **61**, 074024 (2000); G. Buchalla, G. Hiller and G. Isidori, Phys. Rev. D **63**, 014015 (2000); F. Kruger, L. M. Sehgal, N. Sinha and R. Sinha, Phys. Rev. D **61**, 114028 (2000) [Erratum-ibid. D **63**, 019901 (2001)]; F. Kruger and J. Matias, Phys. Rev. D **71**, 094009 (2005).
 - [18] T. Aaltonen *et al.* [CDF Collaboration], Phys. Rev. Lett. **108**, 081807 (2012).
 - [19] O. Seon, Y. J. Kwon, T. Iijima, I. Adachi, H. Aihara, D. M. Asner, T. Aushev and A. M. Bakich *et al.* [Belle Collaboration], Phys. Rev. D **84**, 071106 (2011).
 - [20] J. P. Lees *et al.* [BABAR Collaboration], Phys. Rev. D **85**, 071103 (2012).
 - [21] R. Aaij *et al.* [LHCb Collaboration], Phys. Rev. Lett. **108**, 101601 (2012).
 - [22] K. W. Edwards *et al.* [CLEO Collaboration], Phys. Rev. D **65**, 111102 (2002).
 - [23] Charge conjugation is implied throughout except as explicitly noted.